Annals of Nuclear Energy 69 (2014) 344–351

Contents lists available at ScienceDirect

Annals of Nuclear Energy

journal homepage: www.elsevier.com/locate/anucene

# CFD study of flow accelerated corrosion in 3D elbows

H.P. Rani [a,*], T. Divya [a], R.R. Sahaya [b], Vivekanand Kain [c], D.K. Barua [b]

[a] Department of Mathematics, NIT Warangal, India
[b] Nuclear Power Corporation of India Limited, NU Bhavan, Anushakti Nagar, Mumbai, India
[c] Material Science Division, Bhabha Atomic Research Center, Mumbai, India

ARTICLE INFO

*Article history:*
Received 22 June 2013
Received in revised form 18 January 2014
Accepted 22 January 2014
Available online 18 March 2014

*Keywords:*
Flow accelerated corrosion
Turbulent
Vortex coreline
Helicity
Wall shear stress
Mass transfer coefficient

ABSTRACT

The objective of this paper is to examine the last step of the mechanistic model of wall thinning degradation mechanism i.e., convective mass transfer in feeder pipes under different environments of nuclear power plants (NPP). In the present study, the flow and mass transfer of demineralised water in carbon steel pipes such as single and double elbow was simulated under Indian NPP feeder water system conditions. The numerical simulations of mass transfer results are compared with the wall thickness measurement data of feeder pipes of Indian and CANDU NPP. The eddy structures and their interactions with the wall and the formation of vortex corelines were examined to analyze the flow changes in double elbow pipe. These vortex corelines appeared at the downstream of the bends. The intensity of these vortex corelines has been calculated by plotting the helicity along the vortex coreline. Due to the formation of vortex corelines and resulting flow changes, the mass transfer coefficient (MTC) varies circumferentially. MTC is the most important parameter to predict the highly susceptible FAC locations. For the MTC analysis, the Chilton–Colburn analogy in terms of wall shear stress was used. From this analogy, the effecting behavior of flow and geometrical parameters such as Reynolds number (Re) and the close proximity of bends, respectively, on MTC are studied. The locations of maximum MTC are calculated for both the single elbow of 73° and 90° and the double elbow of 90° and are shown in terms of contours. The flow singularity exists at the elbows; specifically in the double elbow, the downstream elbow is more vulnerable to FAC. The amplified Re results the increased MTC. The close proximity effect, calculated for the vertical limb heights from 0.01 m to 0.65 m, observed to be decrease with the increase of limb height. The changes in the angle of bend, varies the local maximum MTC locations. These reported results are useful for developing the targeted inspection plans in predicting the vulnerable FAC locations.



## 1. Introduction

FAC is a degradation mechanism and is usually encountered in carbon steel piping at certain operating conditions in nuclear power plants (NPP). This phenomenon is possible in the primary and secondary circuits of NPPs. Even though piping in the secondary side is especially susceptible, the carbon steel piping in the primary side of pressurized heavy water reactors (PHWR) also gets affected (Singh et al., 2012; Roychowdhury et al., 2012). Hence in the present study an attempt is made to consider one such critical geometry, namely, the double elbow and the nature of flow under the FAC conditions is analyzed in it. The FAC is a complex phenomenon, in which the mass transfer under the turbulent flow, chemical reactions at the interfaces and mass diffusion in oxide scales are co-operatively or competitively interact with each other. Usually piping with high water flow speeds has the FAC rates exceeding 0.0001 m/year at some locations and one of them is in elbows (Pietralik and Smith, 2006).

Several catastrophic failures have been reported at several power plants around the world since 1981 due to FAC (Kanster et al., 1990). At Surry Unit 2 power plant in 1986 severe elbow rupture happened at the downstream of T-bend and caused 4 fatalities. At Millstone 3 in 1990 failure occurred at the downstream of control valves, caused the failure of two parallel trains but no injuries. At Louviisa-1 in 1990 failure occurred at the downstream of feeder water systems, without injuries. At Prairie Power Plant in 1995, FAC failure occurred at the downstream of T-bend caused the two fatalities. At Fort Colhoun in 1997 failure occurred at the bend, but no injuries. At Mihama 3 in 2004 failure occurred at the downstream of orifice, caused five fatalities and several injuries. Very recently, at Iatan fossil power plant in 2007 failure occurred at downstream of control valve, caused the two fatalities and a huge capital of plant loss (Ahmed, 2010).

* Corresponding author. Tel./fax: +91 0870 2452834.
*E-mail address:* hprani@nitw.ac.in (H.P. Rani).

http://dx.doi.org/10.1016/j.anucene.2014.01.031
0306-4549/

The Surry unit 2 fatal accidents resulted much increased interest in the FAC, particularly in high energy piping and NPP systems. The repeated inspections in NPP have shown that piping components located at the downstream of flow singularities or flow restricting channels or flow redirecting channels, such as sudden expansion or contractions, orifices, valves, T-bend and elbows are most susceptible to the FAC damage. As pointed out by Ahmed (2010), this is due to the severe changes in the flow direction as well as the development of secondary flow instabilities at the downstream of these singularities.

The FAC is strongly influenced by the fluid velocity, wall shear stress, water chemistry, temperature, piping configuration and alloy content (Kain et al., 2008; Kang and Jo, 2008). Also the Mass transfer coefficient (MTC) is the most important flow parameter that affects the FAC and it depends on the geometry, flow rate, turbulence, surface roughness, void fraction in two-phase flows and physical properties of the transported species and of the water (Pietralik and Smith, 2006). The flow and mass transfer analysis in feeder bends under the FAC operating conditions was paid attention in the literature (Pietralik and Smith, 2006; Pietralik, 2008; Pietralik and Schefski, 2011). Other than the feeder bends there are several components such as orifice, sudden expansion and T-bend are also getting affected by FAC (Ahmed, 2010; Gammal et al., 2012). The plant and laboratory (experimental) evidence for the relationship between the local mass transfer conditions and the FAC rate were presented in this analysis. Also the correlations between the MTC in piping components that are highly susceptible to FAC was paid attention.

Fingjun et al. (2008) used the MTC to predict the locations susceptible to FAC and it is correlated with the shear stress distribution. Kang and Jo (2008) used the wall shear stress analysis to predict the thinning behavior by simulating the flow fields inside the feeder pipes of different angles using the commercially available computational fluid dynamics (CFD) software. Gammal et al. (2012) presented the flow and mass transfer analysis at the downstream of an orifice under the FAC conditions. They correlated the FAC rate with the turbulence kinetic energy and mass transfer in terms of Sherwood number (Sh).

Apart from the feeder bends, the steam generator (SG) components are also subjected to corrosive solutions in the turbulent flow and under such conditions the lifetime may be significantly reduced from their original design life time. Pietralik and Heppner (2008) conducted a susceptibility analysis of FAC for tube supports in the recirculating SGs. The ranking of SG locations in the order of FAC susceptibility was estimated from an empirical and Kastner–Riedle model. The effect of local wall thinning on the collapse behavior of pipe elbows subjected to a combined internal pressure and in-plane bending load is investigated by Kim et al. (2008). They evaluated the global deformation behavior of these elbows, which contain various types of local wall-thinning defects at their intrados or extrados. Kain et al. (2008) studied the FAC degraded components from NPP in India and explained the remedial measures for the replacement and possible design and water chemistry changes to combat it. They explained the operating parameters such as the pH and the steel containing Cr that help in minimizing the FAC to offer longer life under similar operating conditions.

From the above studies, it can be observed that most of the earlier numerical studies try to understand about FAC phenomenon in the feeder bends of CANDU NPPs. Hence, an attempt has been made in this study to analyze the flow behavior and degradation phenomenon in feeder pipes (i.e., elbows) of Indian NPP. In these geometries, the significant rheological changes occur under the FAC conditions. The geometries are assumed to be made of carbon steel material and the flow is analyzed at the moderate Re with constant temperature, Schmidt number (Sc) and surface roughness values. The main objective of the present study that followed the experimental inspections of wall thinning locations in 90° bend of Indian NPP and 73° bend of CANDU NPP done by Slade and Gendron (2005) with the emphasis on the exploration of MTC. Further, the FAC effects in this component in terms of varying Re values and in the proximity of the bends are analyzed. These reported results gain currency in predicting the local regions of the pipe that are highly susceptible to FAC and useful for developing targeted inspection plans for the piping components.

In the following sections, a detailed description about the formulation of the problem is given. Also, the governing equations, such as, mass, momentum, energy, turbulence and species transportation equations of the incompressible fluid flow in the considered geometry are shown. Followed by, details about the computational procedure and mesh. Then in the next section, the detailed description of the results in terms of vortex core lines, streamlines, iso-surfaces and contours are presented. Finally, the concluding remarks are made.

## 2. Mathematical formulation

Feeder pipe made of carbon steel material is an integral part of the Main Boiler Feeder Pump Discharge (MBFPD) and High Pressure Heater Discharge (HPHD) line carrying demineralised water from the reactor fuel channels for removing the heat produced by the fission of uranium fuel. The Indian feeder pipe environment has been considered for the FAC analysis. Kang and Jo (2008) did the FAC analysis for the upstream and downstream elbow angles of 30°, 50° and 70°. Under feeder pipe environment, demineralised water flow inside a three-dimensional pipe containing the two right angled (90°) bends schematically presented in the Fig. 1 is considered. Demineralised water flow is assumed to arrive from a circular inlet channel of diameter 0.059 m ($D$) at $x = -0.15$ m. The first and second right angled bends are assumed to be located at 0.15 m and 0.3 m, i.e., at the downstream of the inlet along the $x$-direction and from the first bend along the $y$-direction, respectively. The physical domain of length $-0.15\ \text{m} \leqslant x \leqslant 0.354\ \text{m}$ (6D) was considered to avoid the significant changes in the flow at the inlet and outlet sections of the elbows. It can be observed from Fig. 2 that an increasing length at the downstream for more than 6D (i.e., $x \geqslant 0.354$ m) say, 7D, however, did not change the flow behavior.

The continuity equation along with the Reynolds averaged Navier–Stokes equations, turbulence equations for the turbulence kinetic energy ($k$) and dissipation rate ($\varepsilon$), energy equation and species transport equation have been employed as a mathematical model for an incompressible viscous fluid (demineralised water) passing through a elbow ANSYS Fluent® (2009). The turbulence kinetic energy, $k$ and its rate of dissipation $\varepsilon$, were obtained from the following transport equations of Realizable $k-\varepsilon$ model ANSYS Fluent® (2009).

## 3. The computational procedure and mesh details

The numerical simulation of the governing equations subjected to the boundary conditions were performed by utilizing the commercially available software, namely ANSYS Fluent® (2009). In the first analysis phase, the geometry of the flow model was constructed using the preprocessor, namely ANSYS Design Modeler. The uniform grids were generated and clustered near the bends. This mesh is generated based on the non-dimensional wall distance, $y^+$, which is given by $\sqrt{\frac{\tau_w}{\rho}} \cdot \frac{y}{\nu}$, where $\tau_w$ denotes the wall shear stress. The wall distance between the first calculating node and the wall is chosen to be small, so as to have, $y^+ < 300$ ANSYS Fluent® (2009) based on the following calculations:

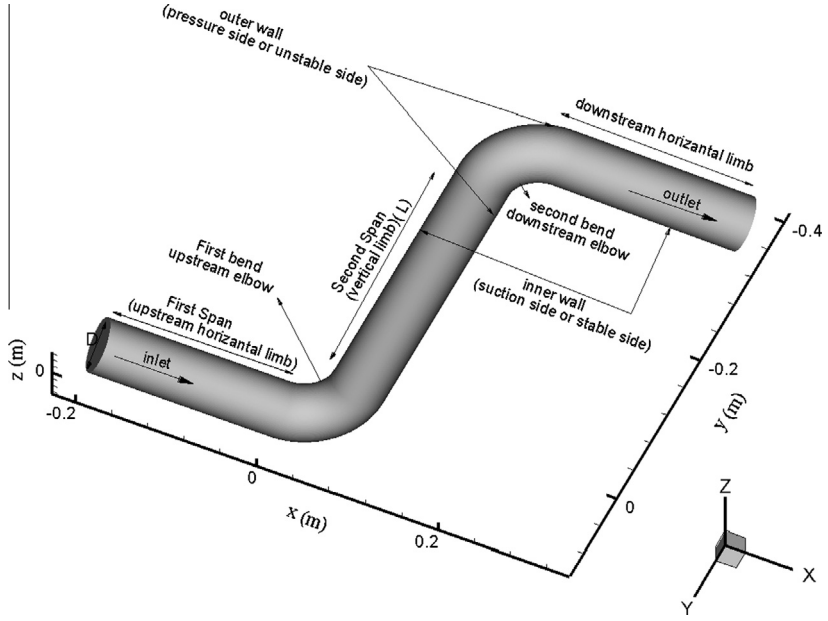


**Fig. 1.** Computational domain of the double elbow.

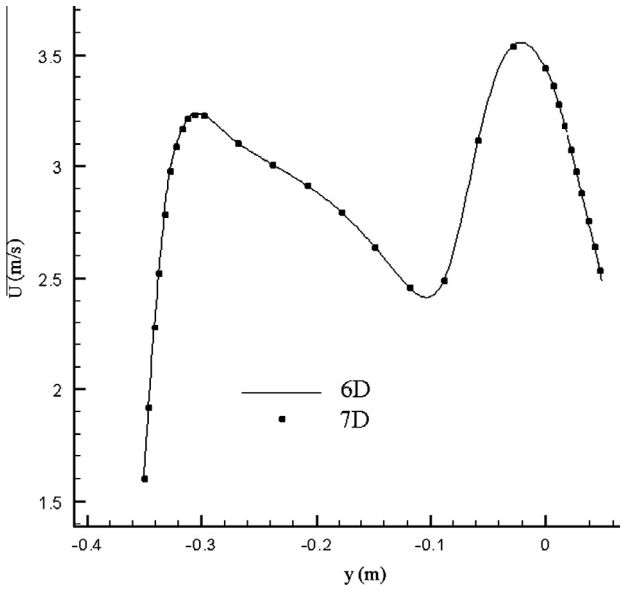


**Fig. 2.** The velocity magnitude (U) in the vertical limb for the different outlet set ups at 6D and at 7D, $D = 0.059$ m.

$$\text{First cell height} = \text{RF}\left[\frac{y^{+}D^{0.125}}{0.199}\left(\frac{\mu}{U_1\rho}\right)^{0.875}\right] \quad (1)$$

where the RF is refinement factor was considered to be 1 to create fine mesh.

The flow volume, boundary and initial conditions for this model had been provided in the ANSYS Fluent® 2009. In the present study, the Indian power plant operating conditions of feeder water system were imposed in the double elbow. The uniform velocity of 3 m/s is used as the inlet boundary condition. No-slip, constant temperature and constant concentration of the species are the boundary conditions imposed on the wall. At the outlet, the zero-gradient properties are considered to be linear for pressure. The FAC conditions of Indian and CANDU NPP considered for the analysis are tabulated in Table 1.

The transitional non-dimensional wall roughness height $k_s^{+}\left(=\frac{\rho k_s u}{\mu}\right)$ is considered to be 2.8, with roughness height $k_s$ of 7.5e−5 (Pietralik and Schefski, 2011). In the above definition $u^{*}$ is represented by $\frac{u}{u^{+}}$ and in the log law layer (as $y^{+} < 450$) $u^{+}$ is defined as $u^{+} = \frac{1}{\kappa}lny^{+} + B$ in which $\kappa$ is the von–Karman's constant (=0.4) and $B = 5.5$ (ANSYS Fluent® 2009; Brown, 1997).

The SIMPLE algorithm was used along with the staggered grid to simultaneously solve the velocity and pressure equations. The POWER LAW scheme was used for discretising convection and diffusion transports on a uniform grid as given in the literature (Debnath et al., 2010). In all the investigations, the iterative calculations of the primitive variables, such as velocity, kinetic energy, rate of dissipation, thermal and species variables were terminated when the residual norm criteria, 1e−7 was reached. The convergence of a solution was also checked from the mass flow summary. The flow imbalance (2.79e−9) was six orders of magnitude smaller than the inflow or outflow (~±6.48e−3). Hence this is a well converged solution in the sense that an imbalance in two to three orders of magnitude smaller than the inflow/outflow typically indicates good convergence. The computations were carried out using the workstation namely, HP Z800 Intel Xeon Dual Core Processor.

Three stages of mesh refinement shown in Fig. 3 were investigated starting with 1767759 nodes, then with 3438083 nodes, and progressing to the final mesh of 6532304 nodes. From Fig. 3, it is observed that the streamwise velocity did not show much variation when the 3438083 nodes were increased by 100% than these nodes were decreased by 50%. Hence, the grid with 3438083 nodes was used for calculating all the results that are presented in this paper. A detailed study of the grid dependence of the present results had not been performed with still finer grids, because it would require a prohibitively large computer capacity.

## 4. Results and discussion

The distribution of flow and local MTC has been analyzed under various operating conditions in Indian NPPs. Also, the flow and geometrical parameters which are affecting the MTC such as Re and the close proximity of bends in the double elbow are analyzed. The flow details are presented in terms of the vortex corelines to

**Table 1**
Indian and Canadian nuclear power plant operating conditions.

| Parameter | Indian NPP (90° bend) | | CANDU NPP (73° bend) |
|---|---|---|---|
| | Single elbow | Double elbow | |
| Outside diameter | 0.3556 m | 0.0635 m | 0.0635 m |
| Thickness | 0.0150876 m | 0.0045 m | 0.0045 m |
| Inner diameter ($D$) | 0.3405124 m | 0.059 m | 0.059 m |
| Radius of curvature | 0.5107686 m | 0.09525 m | 0.09525 m |
| Material | Carbon steel without Chromium content | | Carbon steel with Chromium content of 0.002% |
| Fluid | Demineralized water | | Heavy water |
| Temperature | 150 °C | | 310 °C |
| Schmidt number $\left(\frac{\nu}{D}\right)$ | 9.2 | | 9.2 |
| Reynolds number $\left(\frac{U_1 D}{\nu}\right)$ | 1.016e+6<br>2.032e+6 | 1.761e+5<br>3.523e+5 | 6.27e+6 |

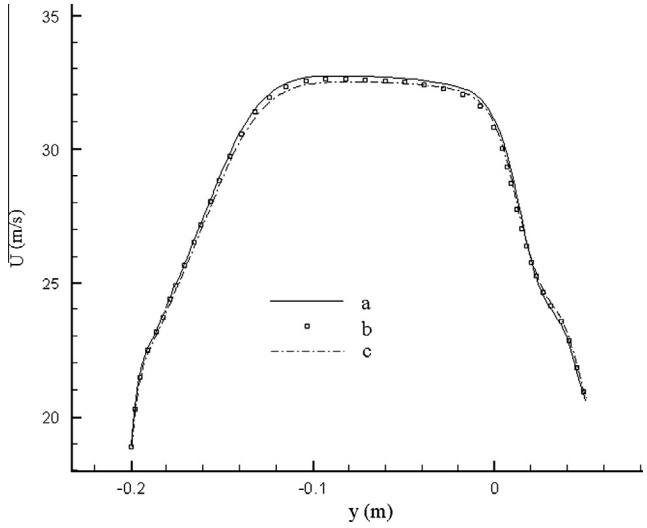


**Fig. 3.** Velocity magnitude (U) with different number of nodes (a) 1767759, (b) 3438083 and (c) 6532304 at $x = 0.059$ m, $-0.238$ m $< y < -0.177$ m, $z = 0$.

study the vortical nature along the double elbow. The MTC distribution is presented in terms of contours to identify the locations which are more susceptible to FAC under the operating conditions.

### 4.1. Vortex core lines and streamlines

Even though the considered component is simple in geometry, the complexities are much beyond our expectations, specifically formation of the spiraling flow. To get further imminent into the vortical flow development in the double elbow, we have plotted the vortical coreline for the global identification of the vortical flow. Roth and Peikert (1998) said that to recognize the vortex and distinguish between the different vortex structures the methods based on extraction of vortex core lines are performed well while other methods based on velocity magnitude, helicity and pressure were poor to perform. From the definition, the entire three dimensional foci span the vortical corelines. Velocity components orthogonal to the vortical coreline are zero at the spiral focal point. The vortical corelines are plotted in Fig. 4 was computed based on the velocity gradient eigenmode method. It could be realize that the fluid particles near the vortical coreline will continue their spiral journey flow in the downwards direction. The spiralling vortex motion had its origin at the bounding walls because the fluid particles near the wall could cause the vortical flow to proceed along the third dimension. Fig. 4(i) shows vortex coreline along with the cross sectional planes which are locally normal to the vortex coreline. Fig. 4(ii) and (iii) shows the streamlines at the cross sectional planes along the vortical corelines in the vertical and horizontal limbs, respectively. The clear observation of these results shows the discriminating changes in the vortex motion along the path of the vortex coreline. It is observed that the system trajectory forms an orbit in the direction of the vortex core. This implies that the kinetic energy along the flow is wrapped around the vortex core. In each cross sectional plane we have observed the spiraling node(N), saddle(S), half node(N′) and half saddle(S′) points and which are satisfying the topological rule i.e., $(N - S) + \frac{1}{2}(N' - S') = 1$ (Tsai and Sheu, 2007).

The vortex nature across the coreline in the vertical limb is discriminated in the four sectional planes (1)–(4) and shown in Fig. 4(ii). Initially at the plane (1) the two counter rotating vortices were observed and originated near the wall region in a symmetric way as the spiraling vortex motion start at the wall. In the downstream region these two counter rotating cells were shifted near the plane of symmetry as shown in planes (2) and (3). Specifically, in the plane (3) near the pressure side or unstable side of the wall two small counter rotating cells were observed at the saddle point of two primary vortices. The vortical behavior in the cross sectional plane (4), shows that the vortex coreline terminated at the wall.

Further, the vortex nature across coreline in the downstream horizontal limb discriminated in the four sectional planes (a)–(d) as shown in the Fig. 4(iii). In the plane (a) the primary vortices are started at the wall. These vortices are divided into two large and two small counter rotating vortices along the symmetry plane as shown in the sectional plane (b). In the downstream flow at the sectional plane (c) the size of secondary vortices was decreased. Further, in the downstream flow at the sectional plane (d), at one side of symmetry plane the small vortex is vanished and at the opposite side the other small vortex gets shortened in size. This nature of different vortex formation shown in Fig. 4, at the cross sectional planes is due to the centrifugal instability (Tsai and Sheu, 2007). This nature of dividing the vortices into small vortices is responsible for the step like axial velocity profile (Soh, 1988).

The intensity of the vortex is described by the parameter helicity, $\phi\left(\equiv \frac{U\cdot\omega}{|U||\omega|}\right)$ (Tsai and Sheu, 2007) and it is plotted along the vortex coreline in Fig. 5. Along with helicity, the velocity gradient $\lambda\left(\equiv \frac{\partial U_s}{\partial_s}\right)$ (Tsai and Sheu, 2007), and pressure also plotted in Fig. 5, where s denotes the unit tangent vector to the vortex coreline. It is observed that $\phi$ is having the higher values at the starting of the vortex coreline (downstream of the first bend) and at the downstream of the second bend. Therefore, the intensity of the spiraling nature is more at the vicinity of first and second bends. Similarly, other parameters, pressure and $\lambda$ have the fluctuations at the downstream of first and second bends.

### 4.2. Mass transfer coefficient

The final step of the degradation mechanism i.e., the convective mass transfer step of ferrous ions from the oxide water interface

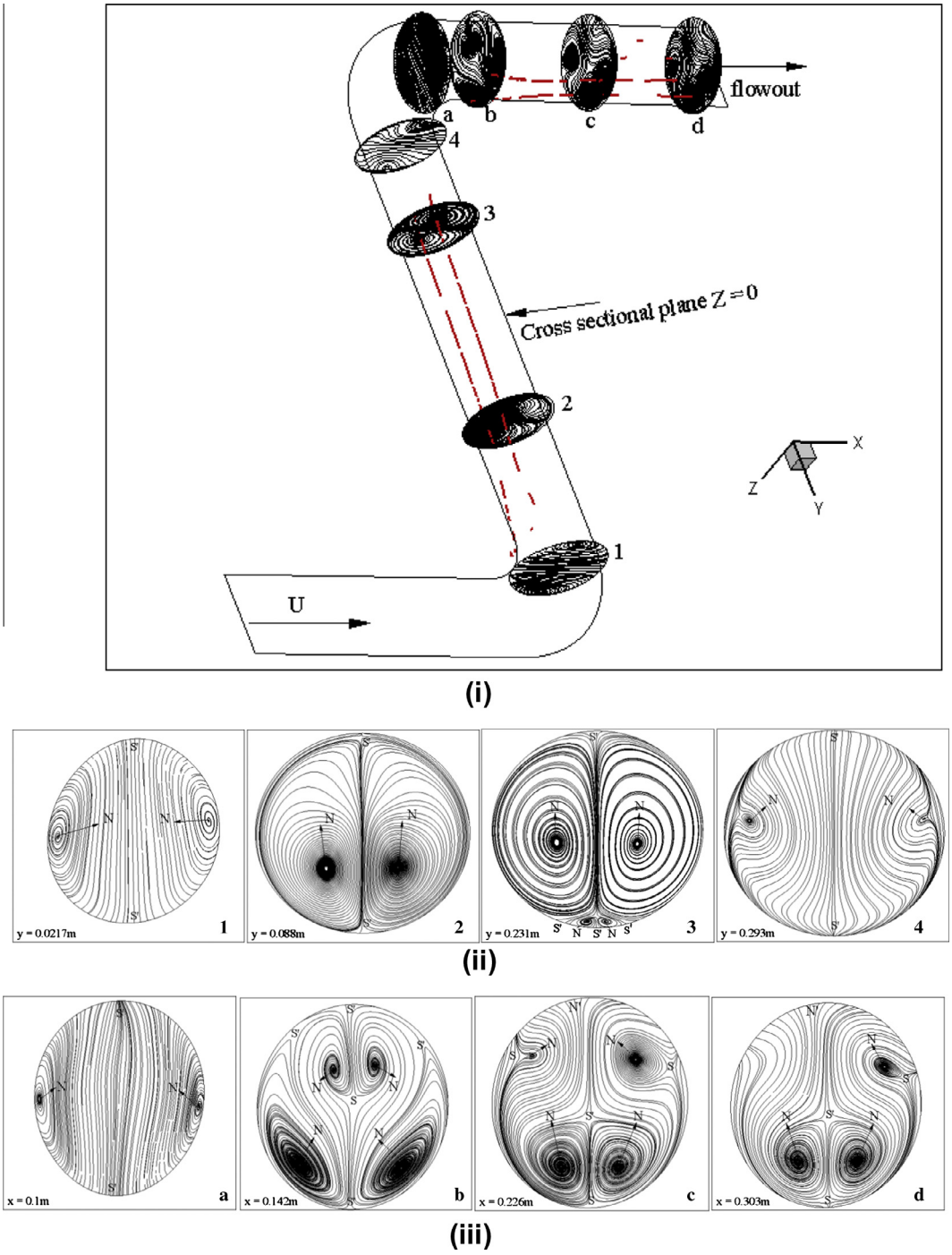


**Fig. 4.** In the double elbow of $L$ = 0.3 m, the simulated streamlines for Re = 1.761e + 5 (i) at different sectional planes which are normal to the vortex coreline (red in color). The sectional planes (1)–(4) are taken in the vertical limb and (a)–(d) are taken in the downstream of horizontal limb. Magnified views of the sectional planes (ii) (1)–(4) are in vertical limb (iii) (a)–(d) are in the downstream horizontal limb. (For interpretation of the references to color in this figure legend, the reader is referred to the web version of this article.)

through the boundary layer of water into the bulk of water was analyzed and is given by

$$F_{fe} = K(C_w - C_b) \tag{2}$$

where $F_{fe}$ is the mass flux of ferrous ions, $K$ is the mass transfer coefficient (MTC), $C_w$ is the concentration of the ferrous ions at the oxide water interface and $C_b$ is the concentration of the ferrous ions in the bulk fluid. For the long piping the mass transfer analysis is not used directly to calculate FAC rate till we know the concentration difference of ferrous ions at the oxide water interface and in the bulk water (Pietralik and Smith, 2006; Pietralik, 2008; Pietralik and Schefski, 2011; Fingjun et al., 2008). But, the concentration difference depends on the first and second step of the thinning degradation mechanism and it is not possible to calculate in the present study. This analysis can be applicable when the piping is short and mass transfer is dominating the FAC rate. In such cases the FAC rate is converted into the proportionality constant, namely, $K$ (Pietralik and Schefski, 2011). The mass transfer coefficient was analyzed extensively to predict the wall thinning locations under operating conditions of Indian and CANDU NPPs. Under the turbulent flow

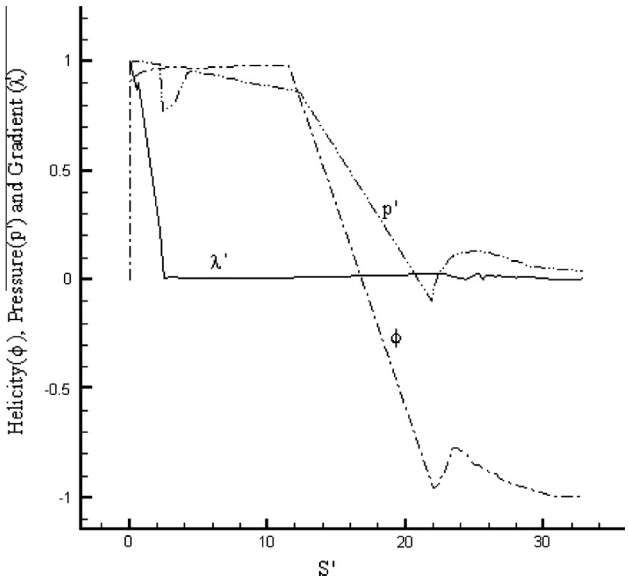


**Fig. 5.** The simulated helicity ($\phi$), normalized pressure ($p'$), and the normalized velocity gradient ($\lambda'$) along the vortex coreline ($S'$).

conditions the MTC (K) was calculated based on the Chilton–Colburn equation (Fingjun et al., 2008). This equation is written in terms of the wall shear stress ($\tau$), mean velocity ($U$), density ($\rho$) and Schmidt number ($Sc$) and is as follows:

$$K = (\tau/U\rho)Sc^{-2/3} \quad (3)$$

The values of $K$ were calculated based on the simulated results of wall shear stress.

#### 4.2.1. For single elbow

Figs. 5 and 6 show the validation of Chilton–Colburn equation for the elbows of angles 73° and 90° under the conditions given in Table 1. Fig. 6 presents the detailed laboratory wall thickness measured data and the present numerical results of mass transfer for 90° bend. Fig. 6(i) presents the wall thickness data of MBFPD and HPHD line of feed water system from Indian NPP. Fig. 6(ii) presents the mass transfer under the same operating conditions resulting in a distribution of $K$. The similar distribution of minimum wall thickness and maximum MTC occurred in the intrados region of the bend. Similarly, Fig. 7(i) shows the measured FAC rate of the CANDU NPP and Fig. 7(ii) shows the simulated MTC results. From the comparison it is observed that the results of Chilton–Colbourn analogy is in good agreement with measured wall thickness data (Slade and Gendron, 2005). Also the observation made from Figs. 6 and 7 is that the variation in angle of the bend, changes the locations of maximum MTC. From Fig. 7 it can be observed that the maximum MTC occurs at the intrados and also at the extrados. But in the 90° elbow, which is shown in Fig. 6, the maximum MTC occurs only at the intrados. These results enable us to find the regions which are vulnerable to FAC in the corresponding component.

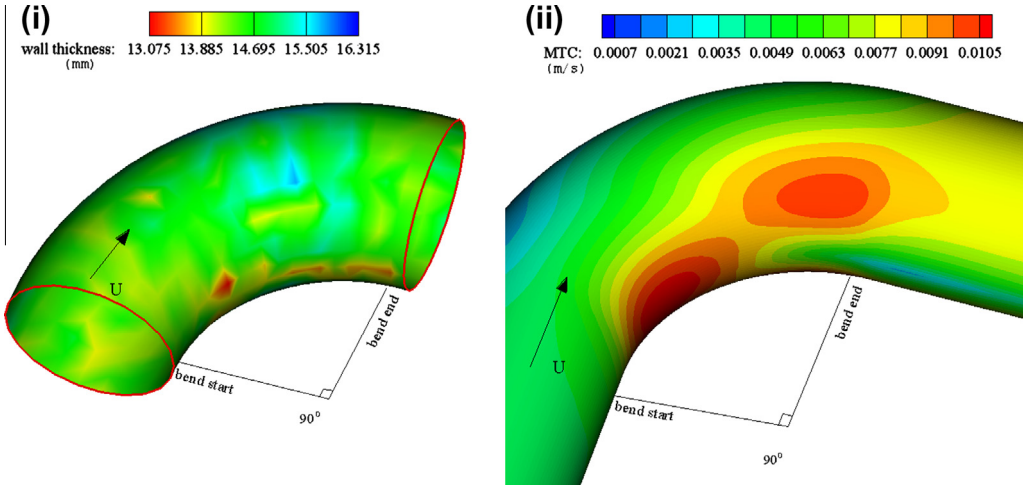


**Fig. 6.** Under the Indian NPP conditions – in 90° bend the contours of (a) measured wall thickness data and (b) simulated MTC.

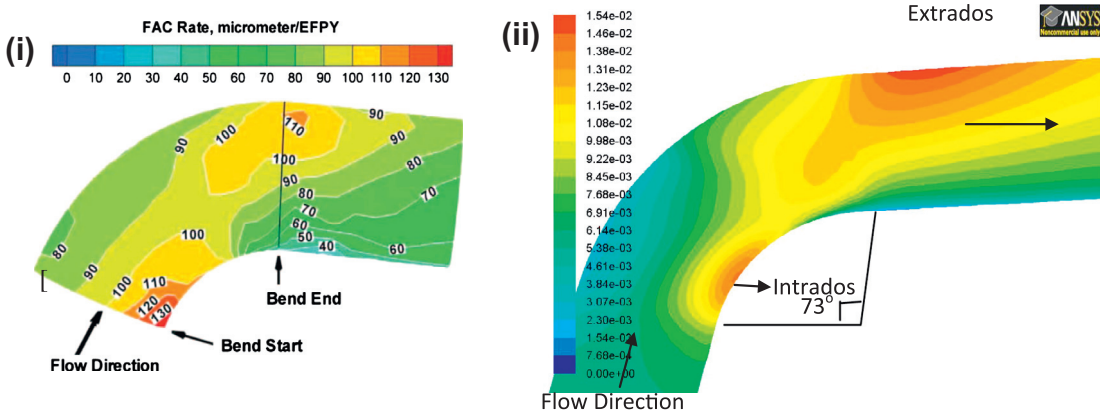


**Fig. 7.** Under CANDU NPP[14] conditions – in 73° bend the contours of (a) measured FAC rate and (b) simulated MTC.

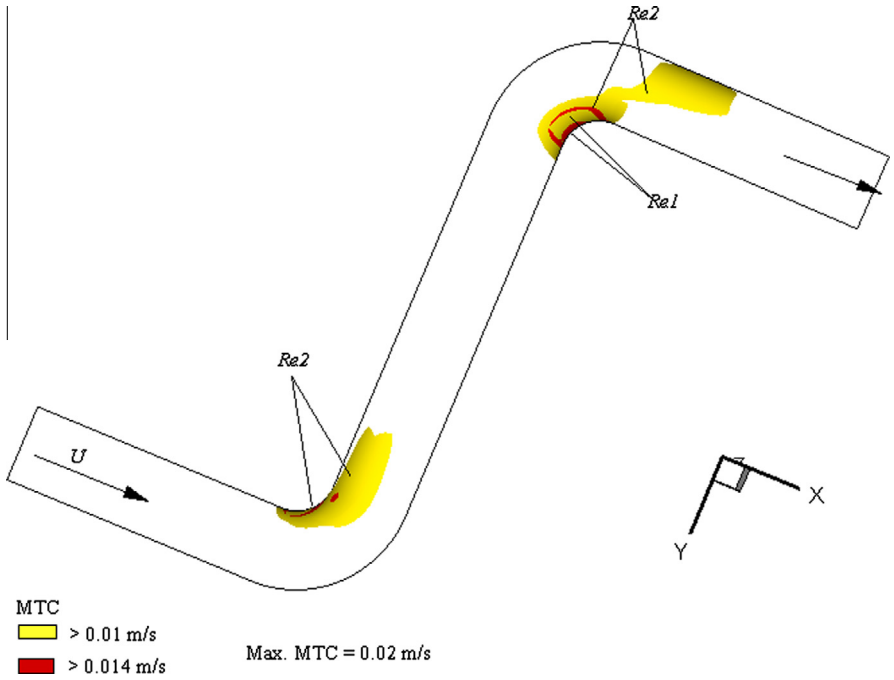


**Fig. 8.** Iso-surfaces of MTC in double elbow for (i) Re1 = 1.761e + 5 (ii) Re2 = 3.523e + 5.

*4.2.2. For double elbow*

In the double elbow pipe the sensitivity studies related to the three different geometrical parameters such as the angles of the first and second bends; the length of the first span between the inlet and the first bend; the length of the second span between the first and second bends (Kang and Jo, 2008) are analyzed. In this study the third parameter which is the length of the second span between the first and second bends is analyzed by fixing other two parameters under the operating conditions as given in Table 1 for the 90° bend. The impact of *Re*, which is affecting the MTC is also analyzed. The iso-surfaces of the MTC have been calculated at two moderate *Re* values, namely, 1.76152e+5(*Re*1) and 3.523e+5(*Re*2) and are shown in Fig. 8. In Fig. 8, the iso-surfaces of the MTC values greater than two fixed values such as 0.01 m/s and 0.014 m/s are shown. It can be observed from Fig. 8 that the maximum MTC in the double elbow pipe is obtained at the bends. The same observations are also made experimentally by Kanster et al. (1990) for the FAC rate in the secondary side of pipe. The regions which are covering above the fixed values of MTC is more for *Re*2 at both the bends and there is no such region exist for *Re*1 at the first bend. Also observed that second bend is getting more affected than the first bend, due to the turbulence created by the first bend (Pietralik and Schefski, 2011). This maximum value of MTC occurred in these two components, such as in the single and double elbows, is due to increase in the local velocity gradient. From Fig. 8, it is observed that increasing *Re* value increases the maximum value of the local MTC.

*4.2.2.1. Close proximity.* In general, for the geometry with close proximity of bends, the downstream bend experiences a higher FAC rate. In the present study, the close proximity effect (CPE) of bends is investigated for fixed *Re* = 1.76152e+5 and for different heights (*L*) of the vertical limb varying from 0.01 m to 0.65 m (i.e., for $L/D < 1$ and $L/D > 1$) using the following correlation of Pietralik and Schefski (2011).

$$\mathrm{CPE} = \frac{MTC_S - MTC_F}{MTC_F} \times 100\% \quad (4)$$

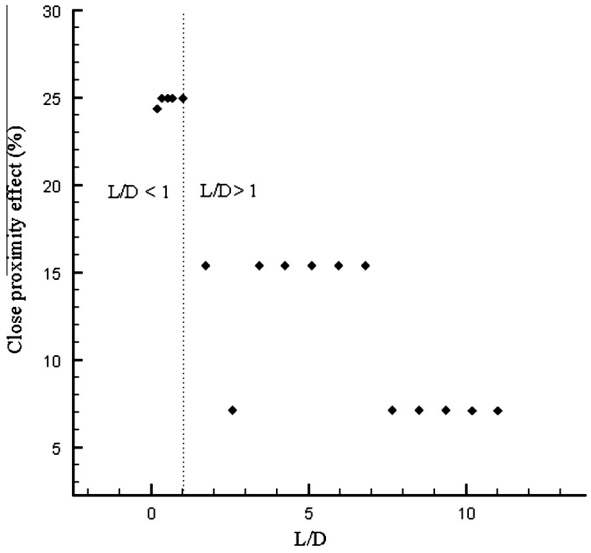


**Fig. 9.** Close proximity effect in double elbow for different heights of vertical limb at Re = 1.761e + 5.

where $MTC_S$ denotes the maximum value of MTC at the downstream bend and $MTC_F$ is the maximum value of MTC at the upstream bend (reference bend). These simulated results are shown in Fig. 9 and it is observed that as the remoteness between the elbows ($L/D$) increases, the CPE is increasing for $L/D < 1$, since the first bend effect is more on the second elbow. As $L/D$ gets amplified ($L/D > 1$) the CPE is constant. This CPE value is lower in comparison with that of $L/D < 1$. This is due to the fact that, when $L/D > 1$, the second bend experiences less impact due to the first bend and, also, there is a fully developed flow between both the bends (Pietralik and Schefski, 2011).

## 5. Conclusions

Computational fluid dynamics was used to calculate and analyze the MTC effects under the FAC operating conditions of Indian

power plants in the double elbow. The vortical flow behavior is captured in terms of vortex coreline. The high intensity of vortex flow motion, fluctuations in the velocity gradient and pressure along the vortex coreline were observed in the vicinity of both the bends. The mass transfer analysis was done using the MTC results. The Chilton–Colburn equation was used to calculate the MTC values from the simulated shear stress values. The validation of the Chilton–Colburn equation was done with the available MTC results in the literature for the single elbow pipe of bend angle 73° and the results are found to be in good agreement. It is observed that the location of maximum MTC in the considered two geometries, namely, single and double elbows, vary with the angle of the bend. In the single elbow (with bend angle 73°) the increased MTC values are located at the intrados and extrados, but in the double elbow (with bend angle 90°) the local maximum MTC is observed at the elbows. This maximum MTC value is due to the increase in the local velocity gradient. In the double elbow, since the first elbow and the second elbow are located in the close proximity to each other, the MTC values at the downstream elbow is more in comparison with that of the upstream elbow. The increase of vertical limb height results the decrease of close proximity effect. These local maximum MTC locations are the locations of maximum FAC rate. The present simulated results will help to identify the locations of high local thinning regions and useful for developing the targeted inspection plans of failure in piping component.

## Acknowledgement

The financial support from the Board of Research in Nuclear Sciences, under BRNS/2009/36/70-BRNS/2390, Department of Atomic Energy is gratefully acknowledged.

## References

Ahmed, W.H., 2010. Evaluation of the proximity effect on flow accelerated corrosion. Ann. Nucl. Energy 37, 598–605.

ANSYS Fluent® version 12.1 Users Guide 2009.

Brown, G.J., 1997. Numerical Simulation of Separated Flows in Three – Dimensional Industrial Geometries: A Case Study. In: Inter Conf on CFD in Mineral & Metal Processing and Power Generation, pp. 157–164.

Debnath, R., Somnath, B., Arindam, M., Roy, D., Snehamoy, M.A., 2010. Comparative study with flow visualization of turbulent fluid flow in an elbow. Int. J. Eng. Sci. Technol. 2 (9), 4108–4121.

Fingjun, L., Lin, Y., Li, X., 2008. Numerical simulation for carbon steel flow-induced corrosion in high-velocity flow seawater. J. Anti-Corros. Method Mater. 55 (2), 66–72.

Gammal, M.Al., Ahmed, W.H., Ching, C.Y., 2012. Investigation on wall mass transfer characteristics downstream of an orifice. Nucl. Eng. Des. 242, 353–360.

Kain, V., Roychowdhury, S., Mathew, T., Bhandakkar, A., 2008. Flow accelerated corrosion and its control measures for the secondary circuit pipelines in Indian nuclear power plants. J. Nucl. Mater. 383, 86–91.

Kang, D.G., Jo, J.C., 2008. CFD application to the regulatory assessment of FAC-caused CANDU feeder pipe wall thinning issue. J. Nucl. Eng. Technol. 40 (1), 37–48.

Kanster, W., Erve, M., Henzel, N., Stellwag, B., 1990. Calculation code for erosion corrosion induced wall thinning in piping system. Nucl. Eng. Des. 119, 431–438.

Kim, J.W., Na, M.G., Park, C.Y., 2008. Effect of local wall thinning on the collapse behavior of pipe elbows subjected to a combined internal pressure and in-plane bending load. J. Nucl. Eng. Des. 238, 1275–1285.

Pietralik, J.M., Heppner, K.L., 2008. Flow-accelerated corrosion susceptibility prediction of recirculating steam generator internals. In: Proceedings of the 16th International Conference on Nuclear Engineering, ICONE16, May 11–15, Orlando, Florida, USA, ICONE16-48630.

Pietralik, J.M., Schefski, C.S., 2011. Flow and mass transfer in bends under flow-accelerated corrosion wall thinning conditions. J. Eng. Gas Turb. Power 133, 012902-1 to 7.

Pietralik, J.M., Smith, B.A.W., 2006. CFD Applications to Flow Accelerated Corrosion in Feeder Bends. In: Proceedings of the 14th International Conference on Nuclear Engineering (ICONE-14), Miami, FL, pp. 89323.

Pietralik, J.M., 2008. Mass Transfer Effects in Feeder Flow-Accelerated Corrosion Wall Thinning. In: 18th CNS International Conference on CANDU Maintenance, Toronto, November 16–18, CW-33126-CONF-009.

Roth, M., Peikert, M., 1998. A higher order method for finding vortex corelines. In: Proceedings of the IEEE visualization.

Roychowdhury, S., Kain, V., Matcheswala, A., Bhandakkar, A., 2012. Sigma phase induced embrittlement in titanium containing austenitic stainless steel tie-bars in a condenser. Eng. Fail. Anal. 25, 123–132.

Singh, J.L., Kumar, Umesh, Kumawat, N., Kumar, Sunil, Kain, V., Anantharaman, S., Sinha, A.K., 2012. Flow accelerated corrosion of carbon steel feeder pipes, from Pressurized Heavy Water Reactors. J. Nucl. Mater. 429, 226–232.

Slade, J.P., Gendron, T.S., 2005. Flow Accelerated Corrosion and Cracking of Carbon Steel Piping in Primary Water-Operating Experience at the Point Lepreau Generating Station. In: Proceedings of the 12th International Conference on Environmental Degradation of Materials in Nuclear Systems, SaltLake City, UT, pp. 773–782.

Soh, W.Y., 1988. Developing fluid flow in a curved duct of square cross section and its fully developed dual solutions. J. Fluid Mech. 188, 337–361.

Tsai, S.F., Sheu, T.W.H., 2007. Numerical exploration of flow topology and vortex stability in a curved duct. Int. J. Numer. Meth. Eng. 71, 564–582.